

Electrochemical Investigations on a Third Generation Biosensor for Determination of Hydrogen Peroxide Based on Immobilization of Myoglobin on a Novel Platinum Nanoparticle/Carbon Nanotube/Ionic Liquid/Nafion Composite

Ali Babaei^{1,2,*}, David J. Garrett², Alison J. Downard^{2,*}

¹ Permanent address: Department of Chemistry, Faculty of Science, Arak University, Arak 38156-8-8349, Iran

² MacDiarmid Institute for Advanced Materials and Nanotechnology, Department of Chemistry, University of Canterbury, Private Bag 4800, Christchurch 8140, New Zealand

*E-mail: a-babaei@araku.ac.ir; Alison.downard@canterbury.ac.nz

Received: 22 February 2012 / Accepted: 19 March 2012 / Published: 1 April 2012

A novel composite film based on platinum nanoparticles (PtNPs), multi-walled carbon nanotubes (MWCNTs), room temperature ionic liquid (RTIL) and Nafion, is an effective matrix to immobilize myoglobin (Mb). Platinum nanoparticles were deposited on MWCNTs and characterized by scanning electron microscopy (SEM) and energy dispersive X-ray spectroscopy (EDS) techniques. Direct electrochemistry and electrocatalysis of Mb were studied in detail using differential pulse voltammetry (DPV), cyclic voltammetry (CV) and chronoamperometry (CA) methods. Using CA, the mediator-free biosensor response was linear with hydrogen peroxide (H₂O₂) concentration in the range of 0.5 to 210 μM with a detection limit of 0.1 μM.

Keywords: Hydrogen peroxide, Platinum nanoparticle, Biosensor, Myoglobin, Ionic liquid

1. INTRODUCTION

There has been considerable interest in achieving direct electrochemistry of proteins on electrode surfaces [1,2]. This effort is aimed at better understanding metabolic processes, constructing biosensors and biofuel cells. However, direct electron transfer between proteins and unmodified electrode surfaces may be difficult due to several factors: the electroactive centres may be embedded deeply in the protein structure, impurities can degrade the response, and the protein often adopts

unfavourable orientations at the electrode [3]. In order to study direct electrochemistry of proteins, modification of the electrode surface is usually necessary.

Fabrication of biosensors based on nanomaterials has attracted the attention of many research groups. These biosensors have advantages such as preserving the activities of the enzyme or protein as well as facilitating direct electron transfer between the biomolecule and the underlying electrode [4,5]. In addition such biosensors can show high stability and good sensitivity in electrochemical applications [6]. In order to enhance electrochemical properties of biosensors much effort has been directed towards investigations of different nanomaterials [7]. Among nanomaterials, carbon nanotubes are an ideal candidate for the construction of biosensors [8]. Carbon nanotubes (CNTs) have unique geometrical, mechanical, electronic and chemical properties [9] which make them extremely attractive for the task of biosensing [10,11]. In order to increase electrocatalytic activity, there is a recent trend toward application of nanomaterials such as platinum [12], silver [13] and gold [14] nanoparticles with based carbon nanotube biosensors. Many factors can affect the electrocatalytic activity of platinum particles, such as particle size and dispersion, support materials, preparation methods, etc [15]. Use of support materials with high surface areas (such as CNTs) is essential to reduce the platinum loading while keeping the high catalytic activity.

Myoglobin (Mb) is a heme protein that plays an important role in oxygen transport in mammals [16,17]. Mb is an attractive candidate for biosensing due to its low cost, commercial availability, well-known structure and its enzyme-like activity. Several studies on direct electrochemistry of Mb have been undertaken [18]. Mb immobilized on a modified electrode surface has shown good electrocatalytic activity for hydrogen peroxide (H_2O_2) reduction [19]. Determination of H_2O_2 is of great importance due to its roles in industry, food, biology, enzymatic reactions, environmental and pharmaceutical research [20,21]. Therefore, it is important to design a sensitive method for rapid, accurate, and reliable determination of H_2O_2 with a low detection limit and wide linear dynamic range.

Nafion is a very widely used polymer with high chemical and mechanical stability and biocompatibility. These properties have led to its use as a membrane material in chemicals and biosensors where it can function to immobilize components, prevent access of interferents to the sensor surface and/or protect the sensor from fouling [22]. Room temperature ionic liquids (RTILs) have been combined with Nafion membranes to give improved material properties. They have been shown to increase the conductivity of the membrane and at the same time, the Nafion membrane effectively immobilizes the IL on the surface [23]. ILs as solvents have attractive properties such as high conductivity, good chemical stability and low volatility. Proteins have been found to maintain their electroactivity in ILs [24,25] and hence a Nafion-IL composite is an interesting immobilization matrix for the construction of electrochemical biosensors [26].

In this work we present direct electrochemistry of Mb on a glassy carbon electrode modified with a novel composite film incorporating Nafion, a RTIL, platinum nanoparticles (PtNPs) and multi-walled carbon nanotubes (MWCNTs). Fabrication and characterization (using scanning electron microscopy (SEM) and energy dispersive X-ray spectroscopy (EDS)) of electrodeposited PtNPs is presented and the effect of PtNP deposition charge on the direct electrochemistry of Mb is investigated. The electrochemistry of Mb in the biosensor is characterized and finally the utility of the biosensor for detection of H_2O_2 is demonstrated.

2. EXPERIMENTAL

2.1. Reagents and Solutions

Mb was obtained from Sigma chemical company. Nafion (NAF) (5 wt% solution in mixture of lower aliphatic alcohols and water) was purchased from Aldrich. The ionic liquid (IL)1-butyl-3-methyl-imidazolium chloride (BMIMCl), multi-walled carbon nanotubes (MWCNTs) (>95 wt%, 5-20 nm diameter), and potassium hexachloroplatinate were obtained from Fluka, PlasmaChem GmbH and Acros companies, respectively. A 50% H₂O₂ solution was purchased from Jasol chemical company and a fresh stock solution of H₂O₂ (0.01M) was prepared daily. All other chemicals were analytical grade and used without further purification. All solutions were prepared using Milli-Q water (>18 MΩ cm). Unless stated otherwise, 0.1 M phosphate buffer (PB), pH 7, was used for the preparation of all standard, sample and measurement solutions.

2.2. Instrumentation

All voltammetric measurements were carried out using a modified glassy carbon electrode (GCE) as a working electrode, a SCE reference electrode and a platinum plate auxiliary electrode. Differential pulse voltammetry (DPV), cyclic voltammetry (CV) and chronoamperometry (CA) experiments were carried out using an Autolab PGSTAT model 302N Potentiostat Galvanostat (EcoChemie, The Netherlands). Rotating disk electrode equipment was from EG&G PARC, model 616 RDE. All potentials are cited with respect to SCE. pH measurements were made with a Hanna model HI8314 pH meter using a combination glass electrode. SEM images and EDS data were obtained using a JEOL 7000F HRSEM with an acceleration voltage of 15 kV.

2.3. Modification of glassy carbon electrodes

A GCE (2.8-mm diameter) was polished using 1.0 and 0.05 μm alumina slurries and rinsed thoroughly with Milli-Q water. The GCE was cleaned by ultrasonic agitation for 5 min in ethanol and then Milli-Q water. The electrode was then dried using a stream of nitrogen gas.

A stock solution of 1 mg mL⁻¹ MWCNTs-DMF was prepared by dispersing 1 mg of MWCNTs in 1 mL dimethylformamide (DMF). 10 μL of MWCNTs-DMF solution was cast on the GCE surface. The electrode was dried at room temperature to obtain MWCNTs/GCE. PtNPs were deposited on MWCNTs/GCE as previously reported [15]. Briefly, the MWCNTs/GCE was placed in the electrochemical cell containing 1.3 mM potassium hexachloroplatinate in 0.5 M sulphuric acid. The PtNPs were deposited by holding the potential at -0.25V for a selected period of time to obtain the selected charge density. A Mb/IL solution was prepared by mixing equal volumes of a 0.2 M aqueous solution of BMIMCl and 10 mg mL⁻¹ Mb solution. 10 μL of the solution was drop coated on PtNPs/MWCNTs/GCE and dried overnight at room temperature. Finally 10 μL of NAF was coated on the modified electrode and dried at room temperature to get the modified electrode denoted as NAF/Mb/IL/PtNPs/MWCNTs/GCE. The modified electrode was stored at 4°C. The UV-Vis data

confirmed the structure of Mb remained intact in the presence of BMIMCl (see supplementary data). This finding is in agreement with a previous report[26]. Other modified electrodes such as NAF/IL/PtNPs/MWCNTs/GCE, NAF/Mb/PtNPs/MWCNTs/GCE and NAF/Mb/IL/MWCNTs/GCE were prepared for comparison, using similar procedures.

2.4 General procedure

A 10 mL solution containing 0.10 M phosphate buffer (pH 7) was transferred into the voltammetric cell. Prior to measurement, electrolytic solutions were purged with highly purified argon gas for at least 30 min, and then an argon atmosphere was maintained over the electrochemical cell during the experiments. Voltammograms were recorded from 0 to -0.65 V. Hydrodynamic chronoamperometry experiments were carried out at 2500 rpm at a potential of -0.25V. The NAF/Mb/IL/PtNPs/MWCNTs/GCE was regenerated by washing the electrode with Mill-Q water between electrochemical measurements. All experiments were performed at room temperature.

3. RESULTS AND DISCUSSION

3.1. SEM and EDS characterization of Pt nanoparticles

To investigate electrochemical formation of PtNPs on the MWCNTs/GCE layer, SEM and EDS measurements were performed.

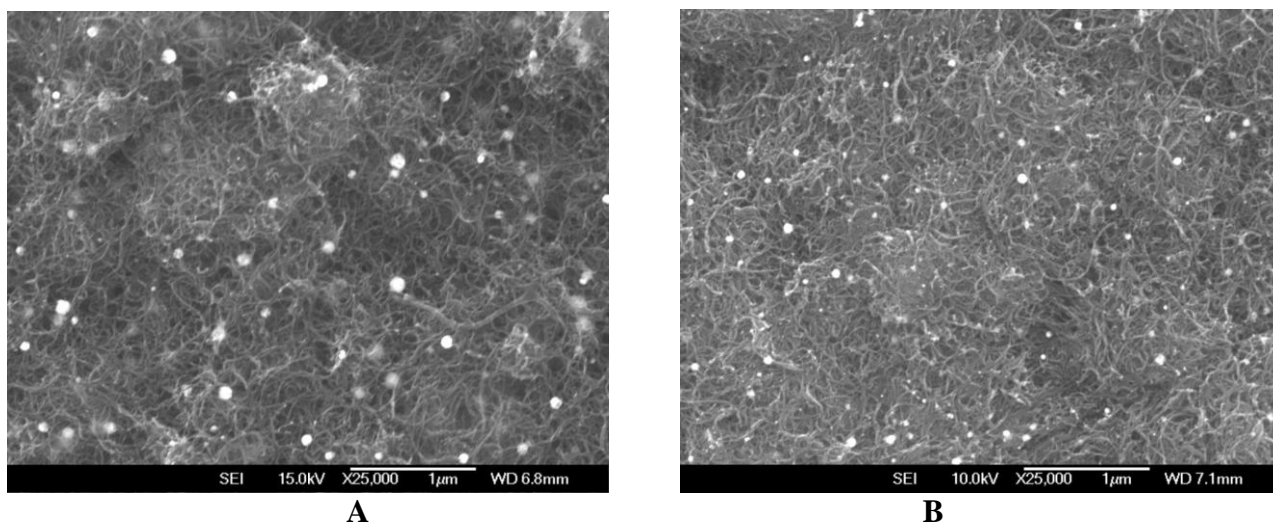


Figure 1. SEM images of PtNPs/MWCNTs/GCE prepared using (A) deposition charge density of $5.2 \times 10^{-3} \text{ C cm}^{-2}$ and (B) deposition charge density of $2.5 \times 10^{-3} \text{ C cm}^{-2}$.

The SEM images of MWCNTs/GCE after electrodeposition of PtNPs are shown Fig.1. Fig. 1A shows PtNPs (with diameters from 90-110 nm) formed at a charge density of $5.2 \times 10^{-3} \text{ C cm}^{-2}$; Fig. 1B

shows PtNPs (with diameter from 40-60 nm) formed at a charge density of $2.5 \times 10^{-3} \text{ C cm}^{-2}$. The PtNPs are electrodeposited uniformly on the porous three-dimensional structure of the MWCNT layer. Increasing charge density leads to a growth in PtNP size. The presence of the PtNPs was confirmed by EDS analysis of MWCNTs/GCE after electrodeposition of Pt (see supplementary data).

3.2. Electrochemical Properties of NAF/Mb/IL/PtNPs/MWCNTs/GCE

Fig. 2 shows the CVs of different modified electrodes in 0.1 M PB (pH 7) at a scan rate of 100 mV s^{-1} in the potential range from 0 to -0.55 V . Voltammogram (a) for NAF/Mb/IL/PtNPs/MWCNTs/GCE shows a pair of well-defined redox peaks ($E_{pc} = -0.44 \text{ V}$ and $E_{pa} = -0.30 \text{ V}$), which can be assigned to the Mb-Fe(III)/Mb-Fe(II) redox couple [14]. Under the same conditions but in the absence of PtNPs, smaller peaks are observed (b). Evidently, the presence of PtNPs enhances the direct electron transfer between Mb and the electrode surface. Voltammogram (c) shows for NAF/Mb/MWCNTs/GCE only very small peaks are obtained for Mb. In the absence of Mb no redox peaks are observed (d).

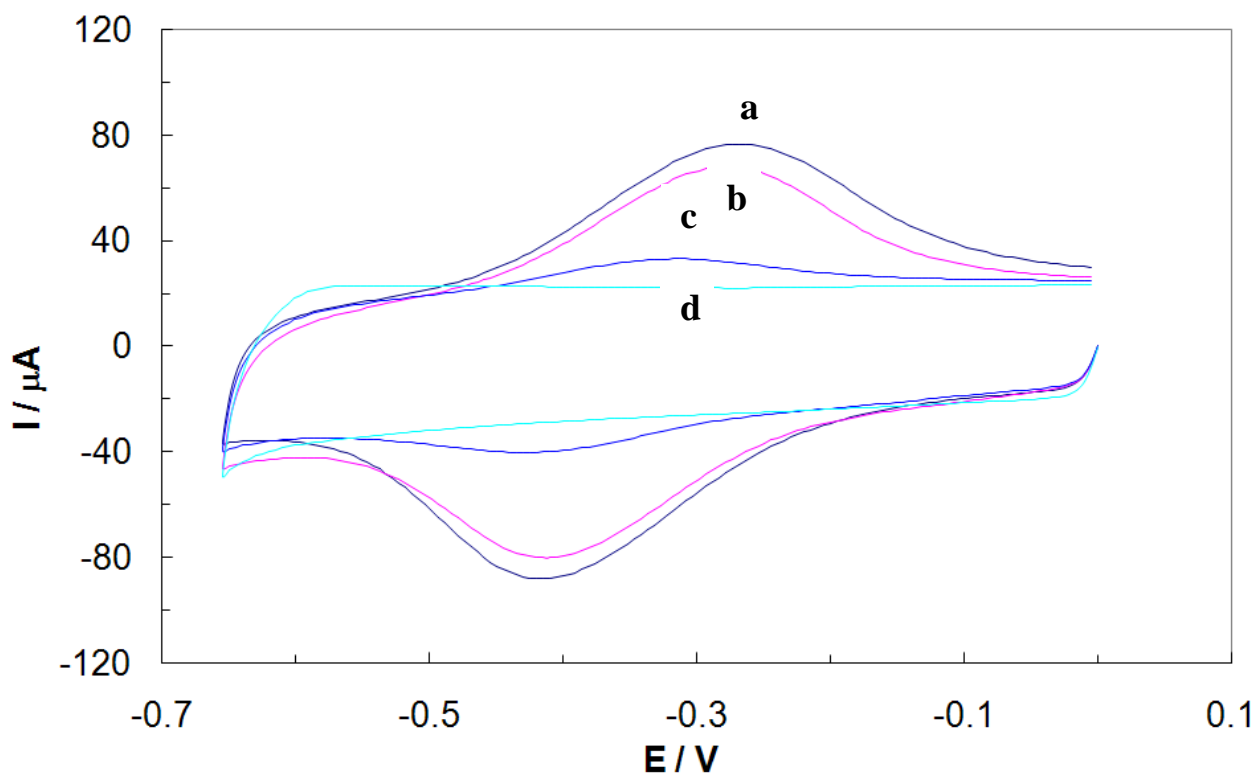


Figure 2. CVs of (a) NAF/Mb/IL/PtNPs/MWCNTs/GCE, (b) NAF/Mb/IL/MWCNTs/GCE, (c) NAF/Mb/MWCNTs/GCE and (d) NAF/IL/PtNPs/MWCNTs/GCE in 0.1M phosphate buffer (pH 7.0) at a scan rate of 100 mV s^{-1} . PtNPs were deposited at charge density of $1 \times 10^{-3} \text{ C cm}^{-2}$.

3.3 Effect of Pt deposition charge

Fig. 3 shows the effect of Pt deposition charge density (based on the geometric area of the GCE) on the cyclic voltammetric anodic peak current of Mb at NAF/Mb/IL/PtNPs/MWCNTs/GCE in PB (pH 7). Increasing the charge density up to $2 \times 10^{-3} \text{ C cm}^{-2}$ increases the peak currents; on further increasing the deposition charge density to $4 \times 10^{-3} \text{ C cm}^{-2}$, the peak currents remain almost constant. This suggests that the PtNPs maintain their activity as their size increases over this deposition charge density range. However with charge densities greater than $4 \times 10^{-3} \text{ C cm}^{-2}$, the peak currents decrease. It appears that the larger particles formed at higher charge densities (Fig. 1) are less active for Mb electrochemistry. These observations are consistent with a previous report on the electrocatalytic activity of PtNPs for oxidation of methanol [15]. A charge density of $3 \times 10^{-3} \text{ C cm}^{-2}$ was chosen for further experiments.

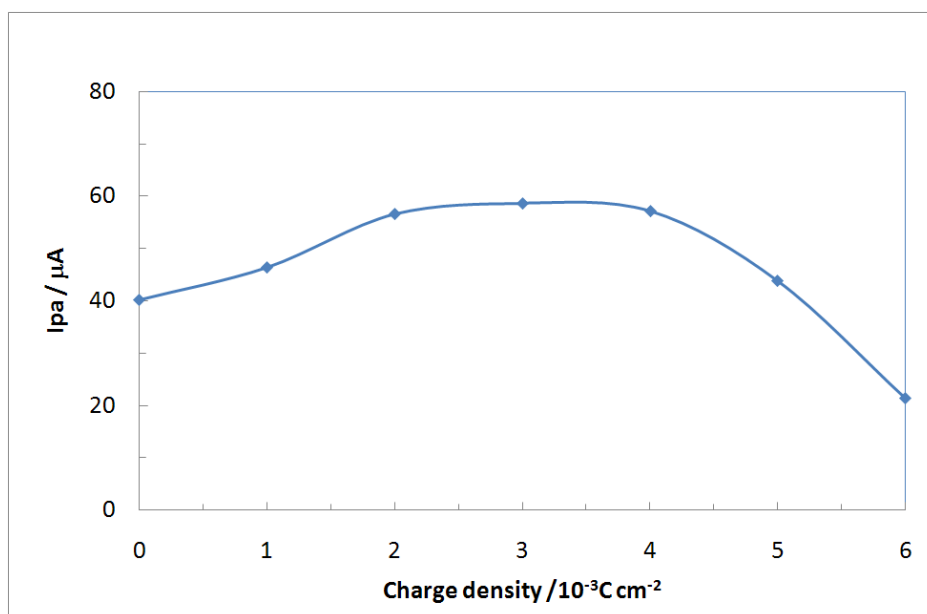


Figure 3. The effect of Pt deposition charge density on CV anodic peak current of NAF/Mb/IL/PtNPs/MWCNTs/GCE in 0.1 M PB (pH 7) at a scan rate of 100 mV s^{-1}

3.4 Influence of scan rate

The effect of potential scan rate on the redox response of Mb at NAF/Mb/IL/PtNPs/MWCNTs/GCE in PB (pH 7.0) was investigated. The CVs are shown in Fig. 4A. The cathodic and anodic peak currents of Mb showed the linear relationships with scan rates between 20 and 200 mVs^{-1} (Fig. 4B), indicating a surface-confined electrochemical process. The linear regression equations for the cathodic and the anodic peaks were:

$$I_{pc} = -560.4 v - 0.498 \quad (R^2 = 0.998)$$

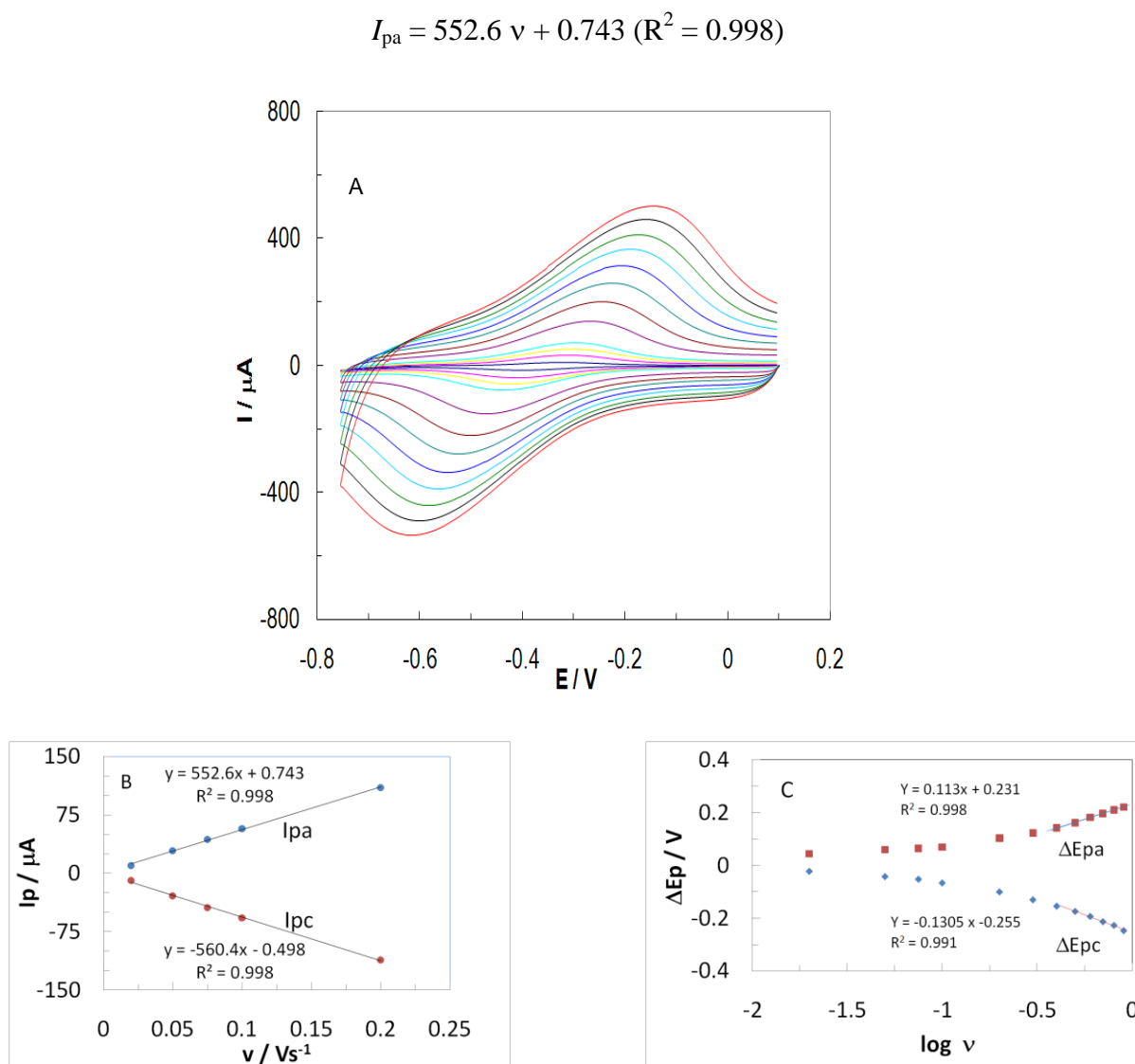


Figure 4. (A) CVs of NAF/Mb/IL/PtNPs/MWCNTs/GCE (deposition charge density of $3 \times 10^{-3} \text{ C cm}^{-2}$) in phosphate buffer at scan rates of $\nu = 20, 50, 75, 100, 200, 300, 400, 500, 600, 700, 800$ and 900 mV s^{-1} , (B) Plot of cathodic and anodic peak currents versus scan rate and (C) plot of relationship between ΔE_p and $\log \nu$ in 0.1 M PB (pH 7).

Fig. 4A shows that the reduction peak shifts negatively and the oxidation peak shifts positively with increasing scan rate, consistent with quasi-reversible electrode kinetics for Mb. Based on Laviron theory [27], the apparent electron transfer rate constant (k_s) and charge transfer coefficient (α) can be determined by measuring the variation of ΔE_p vs. \log scan rate, (ν) (Fig. 4C). Using the relationship:

$$E_p = K - 2.3030 (RT/anF) \log(\nu)$$

and assuming $n = 1$ for Mb, $\alpha = 0.46$ was obtained. Introducing this α value into the following equation, gives $k_s = 0.51 \text{ s}^{-1}$. This value is higher than the previous report ($k_s = 0.41 \text{ s}^{-1}$) [19].

$$\log k_s = \alpha \log(1-\alpha) + (1-\alpha) \log \alpha - \log \left(\frac{RT}{nFv} \right) - \alpha(1-\alpha) \frac{nFE}{2.3RT}$$

3.5 Electrocatalytic reduction of H_2O_2

In order to explore the electrocatalytic activity of Mb on the modified electrode, its response toward the reduction of H_2O_2 was studied. Fig. 5 shows CVs and DPVs of NAF/Mb/IL/PtNPs/MWCNTs/GCE in the presence of various concentrations of H_2O_2 . In the presence of H_2O_2 there is a small reduction peak close to -0.15 V with peak height proportional to H_2O_2 concentration.

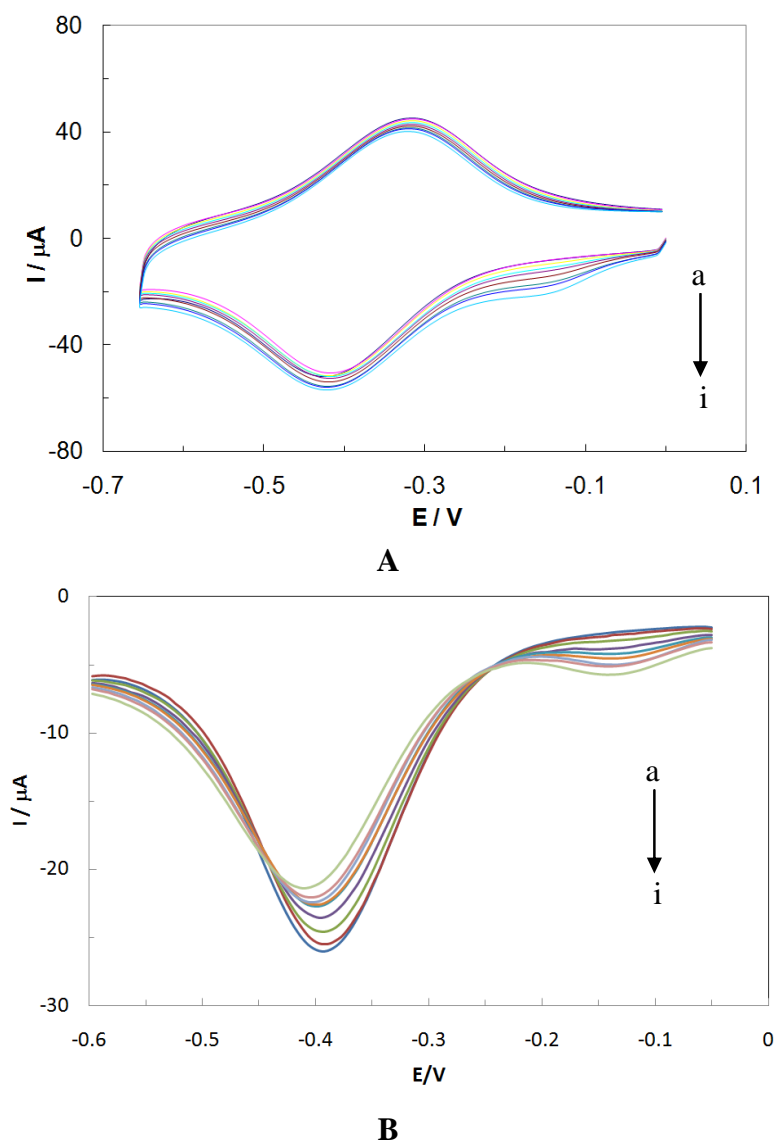
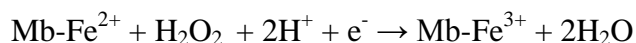
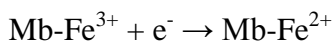
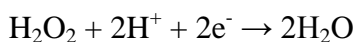


Figure 5. (A) CVs of NAF/Mb/IL/PtNPs/MWCNTs/GCE in the presence of various concentrations of H_2O_2 (a-i): 0, 10, 60, 100, 140, 200, 260, 320 and 400 μM in 0.1 M PB (pH 7) at 50 mV s^{-1} scan rate and (B) DPVs of NAF/Mb/IL/PtNPs/MWCNTs/GCE in presence of various concentrations of H_2O_2 (a-i): 1, 10, 50, 100, 160, 200, 240, 280 and 400 μM in 0.1 M PB (pH 7).

This small peak is assigned to the catalytic reaction described below [28]:



which gives the overall reaction:



The peak occurs before the Mb reduction peak because the second reaction above starts as soon as the first reaction occurs. However, H_2O_2 is depleted in the diffusion layer by the second reaction and hence the catalytic current decreases as the scan proceed, resulting in the ‘prepeak’.

When the measurement was repeated using the NAF/IL/PtNPs/MWCNTs/GCE no reduction peak was observed in absence of Mb (supplementary data). These results confirmed the role of Mb in electrocatalytic reduction of H_2O_2 .

Fig. 6 displays hydrodynamic chronoamperograms obtained at the rotated NAF/Mb/IL/PtNPs/MWCNTs/GCE (2500 rpm) with successive injections of H_2O_2 at an applied potential of -0.15 V in PB (pH 7). Two linear ranges are observed. The first (Fig 6. Inset A) was from 0.5 to 110 $\mu\text{mol L}^{-1}$, with a calibration equation of $I_p(\mu\text{A}) = 0.1023c (\mu\text{mol L}^{-1}) + 0.2324$ ($R^2=0.9941$). The second linear dynamic range (Fig. 6, Inset B) was from 110 to 210 $\mu\text{mol L}^{-1}$, with a calibration equation of $I_p(\mu\text{A}) = 0.0438c (\mu\text{mol L}^{-1}) + 6.38$ ($R^2=0.9921$). A detection limit of 0.1 μM ($S/N = 3$) was obtained. In addition, the modified electrode reached 95% of the steady-state current within 4 s, showing the electrode gives a rapid response. Comparison of these results with previous results as shown in Table 1, indicates the proposed sensor performs well with a relatively low detection limit and wide linear dynamic range.

As can be seen in Fig. 6, when the concentration of H_2O_2 increases above 210 μM , the response decreases and then reaches a plateau. This phenomenon is consistent with Michaelis-Menten kinetics. The apparent Michaelis-Menten constant ($K'm$) can be obtained by the hydrodynamic amperometric method according to the Lineweaver-Burke equation [29], where I_{ss} is the steady state current after addition of the substrate, I_{max} is the maximum current measured under saturated substrate conditions and C is the bulk concentration of the substrate:

$$\frac{1}{I_{ss}} = \frac{K'm}{I_{max}C} + \frac{1}{I_{max}}$$

By analysis of the slope and the intercept of the experimental data plot, the $K'm$ value for the catalytic activity of Mb in NAF/Mb/IL/PtNPs/MWCNTs/GCE for H_2O_2 was determined as 69 μM . This relatively small value (Table 1) shows that the immobilized Mb efficiently catalyses the reduction of H_2O_2 .

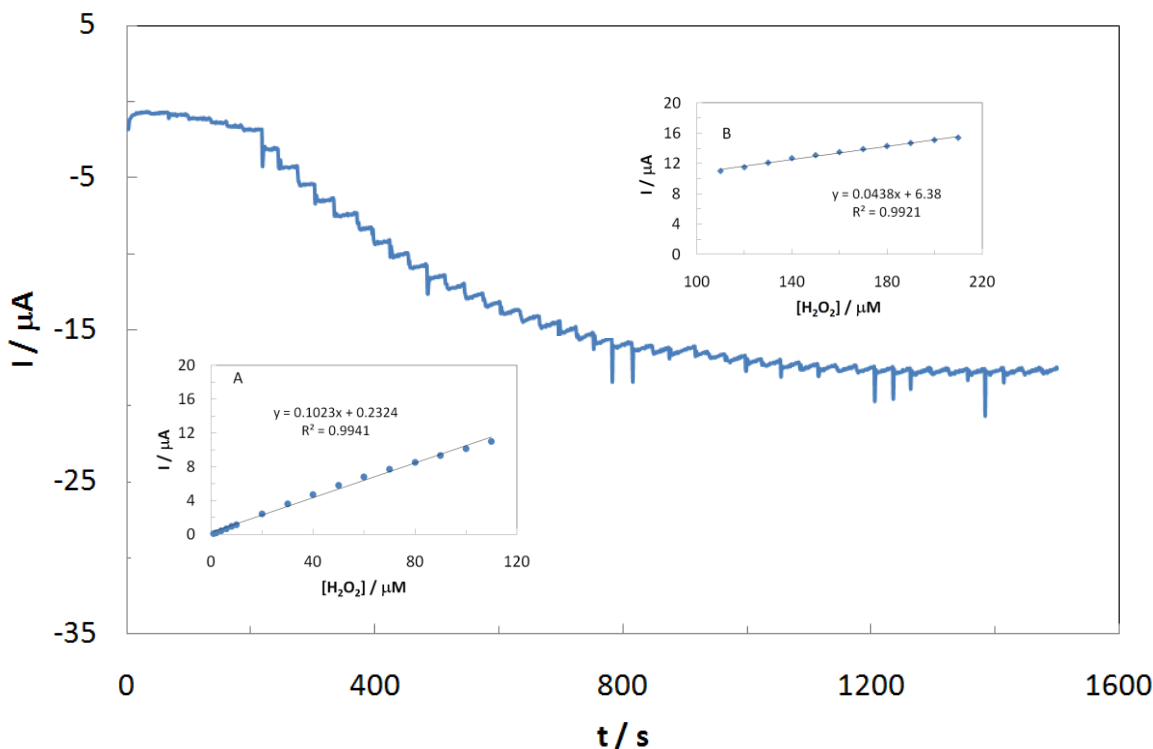


Figure 6. Amperometric responses obtained using NAF/Mb/IL/PtNPs/MWCNTs/GCE at -0.15 V upon successive addition of H₂O₂ in 0.1 M PB (pH 7). The insets show current versus H₂O₂ concentration plots.

Table 1. Comparison of Various Mb-based-modified electrodes for H₂O₂ determination

Electrode	Linear range (μM)	Detection limit (μM)	K'm (μM)	References
Mb/MWCNTs-COL/DMSO/GCE	0.6-39	0.16	106	30
Mb/GNPs/MWCNTs/GCE	2.0-500	0.6	NR	14
Mb-[EMIM][BF ₄]-HA/GCE	2.0-270	0.6	290	31
Mb/CILE	6.0-160	2.0	140	32
Mb-HSG-SN-CNTs/GCE	2.0-1200	0.36	1620	19
Mb/DNA/CILE	1.0-160	0.2	420	33
Mb/Clay-IL/GCE	3.9-259	0.73	17.3	16
NAF/Mb/IL/GCE	1.0-180	0.14	22.6	26
Mb-Chi-ZnO/GCE	2.0-240	0.21	32	28
NAF/Mb/IL/PtNPs/MWCNTs/GCE	0.5-210	0.1	69	This work

Note: Mb, myoglobin; MWCNTs, multiwalled carbon nanotubes; Col, collagen; DMSO, dimethyl sulfoxide;GNPs, gold nanoparticles; [EMIM][BF₄], 1-ethyl-3-methyl-imidazolium tetrafluoroborate; CILE, Carbon ionic liquid electrode; HSG, hybrid sol-gel; SN, Silver nanoparticles;Chi, Chitosan; CNTs, carbon nanotubes.

3.6 Stability, reproducibility, repeatability and selectivity of the NAF/Mb/IL/PtNPs/MWCNTs/GCE

The stability of the NAF/Mb/IL/PtNPs/MWCNTs/GCE composite was studied by repeat CV scans at 100 mVs^{-1} between 0 and -0.65 V . CVs showed only a 2.6% decrease in peak height for Mb after 100 scans, indicating that the sensor components are very stably immobilized on the GCE surface and that Mb electroactivity is not degraded under these conditions. Eight repeat DPV measurements of $150 \text{ }\mu\text{M H}_2\text{O}_2$ using the same electrode gave a relative standard deviation (RSD) of 3.8% confirming excellent repeatability. Electrode-to-electrode reproducibility was also satisfactory. A series of 4 modified electrodes which were prepared individually gave an RSD of 6.8 % for determination of $150 \text{ }\mu\text{M H}_2\text{O}_2$.

The stability of the NAF/Mb/IL/PtNPs/MWCNTs/GCE to storage at 4°C was assessed. The electrode retained approximately 95% and 69% of its sensitivity toward reduction of H_2O_2 , after storage for seven days in air and PB (pH 7), respectively. High stability to storage in air is clearly an advantage for a practical sensor.

The selectivity of the modified electrode was also tested by studying the effects of potential interfering species on the determination of $150 \text{ }\mu\text{M H}_2\text{O}_2$ in PB (pH 7) by DPV technique. After addition of 1.0 mM dopamine, citric acid, glucose and uric acid, the responses of the electrode varied by 2.1, 5.1, 1.9 and 5.5% respectively, demonstrating good selectivity of the biosensor toward determination of H_2O_2 .

4. CONCLUSION

A new biosensor for the determination of H_2O_2 had been constructed, based on immobilization of Mb on a NAF/IL/PtNPs/MWCNTs composite. Our results showed, for the first time, the presence of PtNPs can enhance the electrochemistry of Mb on the modified electrode. The size of the electrochemically deposited platinum nanoparticles was found to affect the activity for Mb electrochemistry. The fabricated modified electrode showed excellent electrocatalytic activity for reduction of H_2O_2 in PB (pH 7). Hydrodynamic chronoamperometry of H_2O_2 on the modified electrode revealed two linear dynamic ranges with the lowest reported detection limit for H_2O_2 determination. The proposed biosensor showed excellent analytical features such as high sensitivity, selectivity, reproducibility and stability with short response time for determination of H_2O_2 . These features suggest that the proposed sensor is an attractive candidate for practical applications.

ACKNOWLEDGEMENTS

A.B. thanks Arak University for a sabbatical fellowship and the Department of Chemistry, University of Canterbury, for supporting this research. D.J.G acknowledges the Tertiary Education Commission for a Top Achiever Doctoral Scholarship. The authors acknowledge Dr Owen Curnow who kindly provide BMIMCl and his useful comments on applications of ILs.

References

1. Y. Zhang, and J. Zheng, *Electrochim. Acta* 54 (2008) 749
2. Q. Zhang, W. Wei, and G.-C. Zhao, *Electroanalysis*, 20 (2008) 1002.
3. J.J. Feng, J.J. Xu, and H.Y. Chen, *J. Electroanal. Chem.*, 585 (2005) 44.
4. H.J. Jiang, C. Du, Z.Q. Zou, X.W. Li, D.L. Akins, and H. Yang, *J. Solid State Electrochem.*, 13 (2009) 791.
5. C.Y. Deng, J.H. Chen, X.L. Chen, C.H. Xiao, L.H. Nie, and S.Z. Yao, *Biosens. Bioelectron.* 23 (2008) 1272.
6. G.Z. Liu, M.N. Paddon-Row, and J.J. Gooding, *Electrochem. Commun.* 9 (2007) 2218.
7. Z.H. Dai, K. Liu, Y.W. Tang, X.D. yang, J.C. Bao, and J. Shen, *J. Mater. Chem.*, 18 (2008) 1919.
8. G.A. Rivas, M.D. Rubianes, M.C. Rodriguez, N.F. Ferreyra, G.L. Luque, M.L. Pedano, S.A. Miscoria, and C. Parrado, *Talanta*, 74 (2007) 291.
9. I. Dumitrescu, P.R. Unwin, and J.V. Macpherson, *Chem. Commun.*, 45 (2009) 6886.
10. C. N. R. Rao, B. C. Satishkumar, A. Govindaraj, and M. Nath, Nanotubes, *Chem. Phys. Chem.* 2(2001) 78.
11. R. H. Baughman, A. A. Zakhidov, and W. A. de Heer, *Science* 297(2002) 787.
12. Y.C. Tsai, S.Y. Chen, and C.A. Lee, *Sens. Actuators: B*, 135 (2008) 96.
13. C.Y. Liu, and J.M. Hu, *Biosens. Bioelectron.*, 24 (2009) 2149.
14. W. Cao, C. Wei, J. Hu, and Q. Li, *Electroanalysis*, 20 (2008) 1925.
15. Z. He, J. Chen, D. Liu, H. Tang, W. Deng, and Y. Kuang, *Mat. Chem. Phys.*, 85 (2004) 396.
16. Z. Dai, Y. Xiao, X.Z. Yu, Z.B. Mai, X.J. Zhao, and X.Y. Zou, *Biosens. Bioelectron.*, 24 (2009) 1629.
17. L. Zhang, D.B. Tian, and J.J. Zhu, *Bioelectrochemistry*, 2008, 74, 157.
18. L. Zhang, Q. Zhang, and J. Li, *Biosens. Bioelectron.* 26 (2010) 846.
19. C.Y. Liu, and J.M. Hu, *Biosens. Bioelectron.*, 24 (2009) 2149.
20. D. Tang, R. Yuan, and Y. Chai, *Electroanalysis*, 18 (2006) 259.
21. J. Wang, Y. Lin, and L. Chen, *Analyst*, 118 (1993) 277.
22. Z. Guo, and S. Dong, *Anal. Chem.*, 76 (2004) 2683.
23. H. Chen, Y. Wang, Y. Liu, Y. Wang, L. Qi, and S. Dong, *Electrochem. Commun.*, 9 (2007) 469.
24. X. Lu, Q. Zhang, L. Zhang, and J. Li, *Electrochem. Commun.*, 8 (2006) 874.
25. Y. Wang, J. Wu, T. Zhan, W. Sun, and K. Jiao, *Sens. Lett.*, 7 (2009) 1106.
26. A. Safavi, and F. Farjami, *Anal. Biochem.*, 402 (2010) 20.
27. E. Laviron, *J. Electroanal. Chem.* 101 (1979) 19.
28. X. Feng, Y. Liu, Q. Kong, J. Ye, X. Chen, J. Hu, and Z. Chen, *J. Solid State Electrochem.* 14 (2010) 923.
29. R. A. Kamin, and G. S. Wilson, *Anal. Chem.* 52 (1980) 1198.
30. S. Zong, Y. Cao, and H. Ju, *Anal. Lett.* 40 (2007) 1556.
31. Y. Zhang, and J. Zheng, *Electrochem. Commun.* 10 (2008) 1400.
32. S. Shangguan, and J. Zheng, *Electroanalysis*, 21 (2009) 881.
33. R. Gao, J. Zheng, *Electrochem. Commun.*, 11 (2009) 1527.

SUPPLEMENTARY FIGURES:

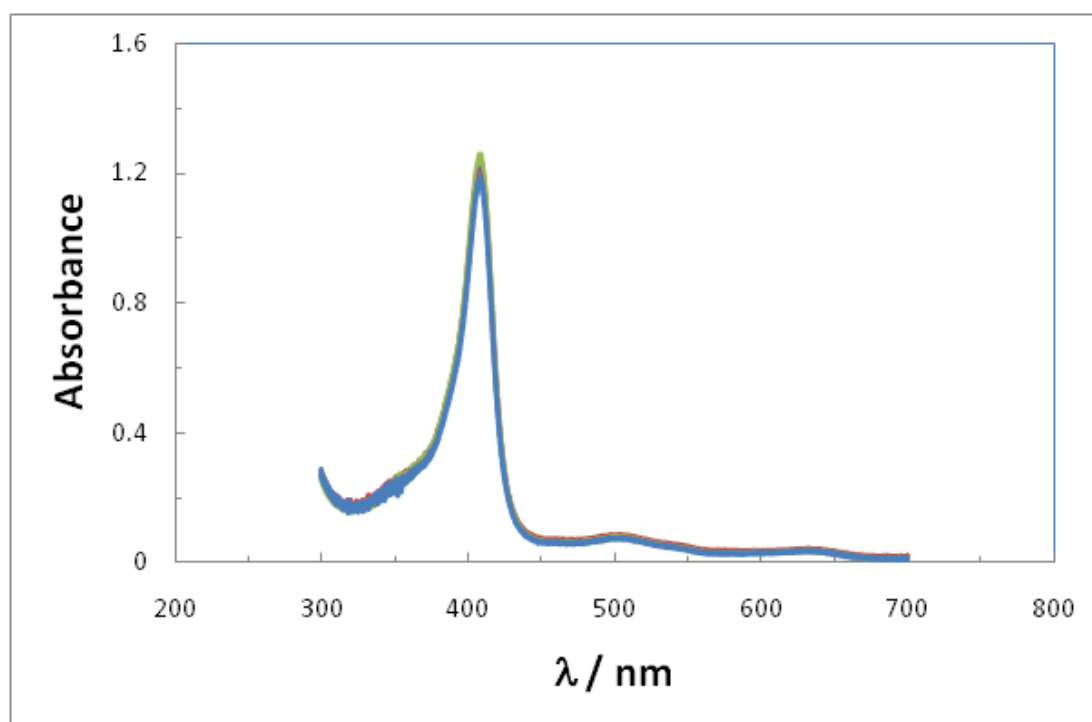


Figure S1. UV-Vis absorption spectra of Mb (1.2×10^{-5} M) in presence various concentrations of BMIMCl from 0 (green) to 0.1M (blue) in PB (pH 7)

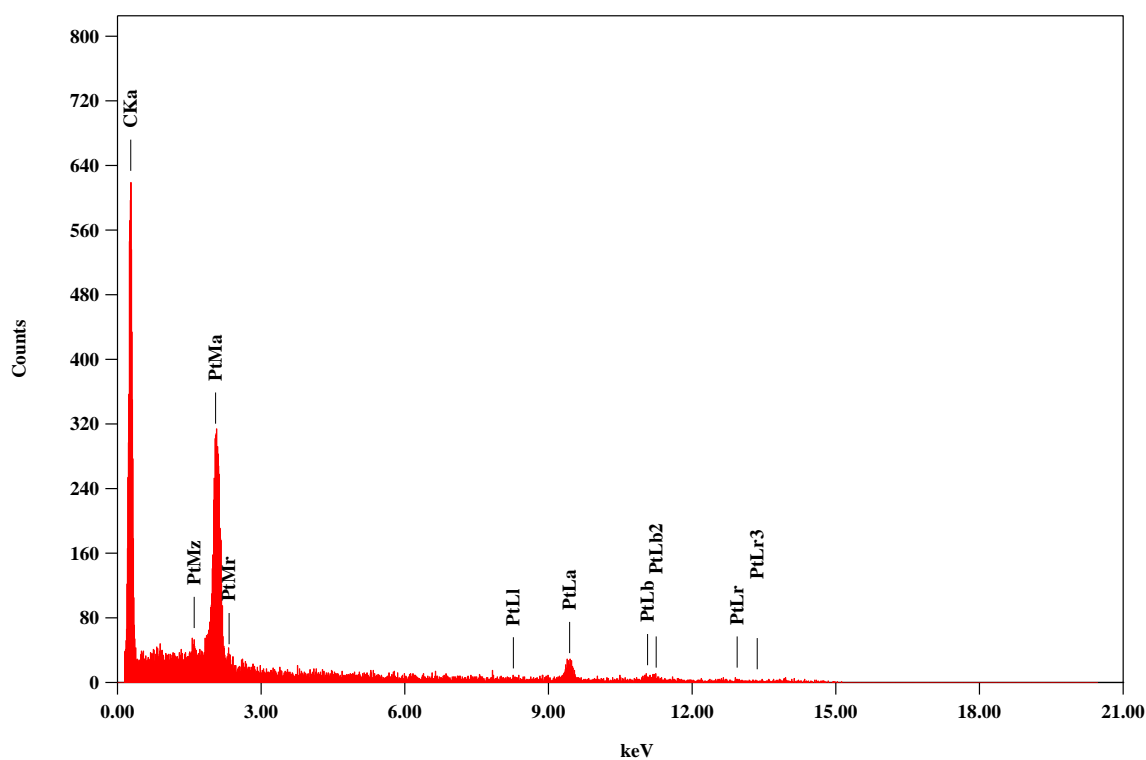


Figure S2. EDS analysis results for PtNPs/MWCNTs/GCE.

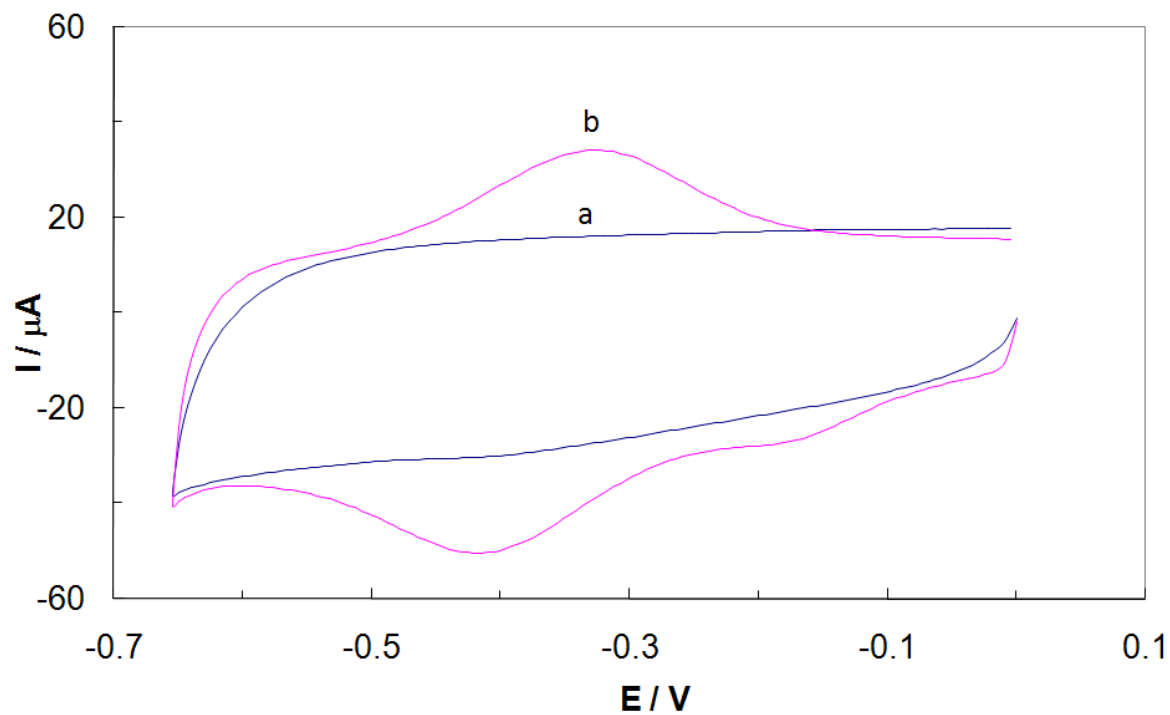


Figure S3. CVs of (a) NAF/Mb/IL/PtNPs/MWCNTs/GCE and (b) NAF/IL/PtNPs/MWCNTs/GCE in presence of 200 μM H_2O_2 and 0.1M phosphate buffer (pH 7.0) at a scan rate of 50 mV s^{-1} .